Analysis of the (100)Si/LaAlO$_3$ structure by electron spin resonance: nature of the interface

K. Clémer · A. Stesmans · V. V. Afanas'ev ·
L. F. Edge · D. G. Schlom

Abstract Electron spin resonance of paramagnetic point defects was used to probe (100)Si/LaAlO$_3$ structures with nm-thick amorphous high-dielectric constant (κ) LaAlO$_3$ layers deposited directly on clean (100)Si by molecular beam deposition at ~100 °C. Unlike common high-κ metal oxide/Si entities, no P$_b$-type interface defects could be observed in the as-grown state, revealing the absence of an Si/SiO$_2$-type interface in terms of these archetypal Si-dangling bond-type Si/SiO$_2$ interface defects (P$_{b0}$, P$_{b1}$). This state is found to persist during subsequent thermal treatment (5% O$_2$/N$_2$ mixture) up to T_{an} ~ 800 °C, indicating a thermally stable abrupt Si/LaAlO$_3$ interface. However, in the range T_{an} ~ 800–860 °C, a Si/SiO$_2$-type interface starts forming as evidenced by the appearance of P$_{b0}$ defects and, with some retardation in terms of T_{an}, the EX center—an SiO$_2$ associated defect, attesting to significant structural/compositional adaptation. Monitoring the defect density versus T_{an} indicates the SiO$_x$ nature of the interlayer to disintegrate again upon heating at $T_{an} \geq 930$ °C, possibly related to intensifying crystallization and silicate formation. Despite intensive search, no LaAlO$_3$-specific point defects could be revealed.

K. Clémer (✉) · A. Stesmans · V. V. Afanas'ev
Department of Physics, University of Leuven, 3001 Leuven,
Belgium
e-mail: katrijn.clemer@fys.kuleuven.be

L. F. Edge · D. G. Schlom
Department of Materials Science and Engineering,
Pennsylvania State University, University Park, PA 16802,
USA

1 Introduction

The unabated down-scaling of Si/SiO$_2$-based complementary metal-oxide-semiconductor (CMOS) transistors will require the replacement [1, 2] of the conventional SiO$_2$ gate dielectric with an alternative gate dielectric of higher dielectric constant (κ). These high-κ dielectrics allow the application of physically thicker films of equivalent SiO$_2$ electrical (capacitive) oxide thickness (EOT) required to be reduced to less than 1 nm for future realization of MOS gate lengths <30 nm [3].

Intensely investigated candidate dielectrics are metal oxides in their simplest form such as HfO$_2$, ZrO$_2$, Al$_2$O$_3$, La$_2$O$_3$ and others, [1, 4] as well as in more complex varieties such as silicates, aluminates, pseudo-binary mixtures and multi metal oxide compounds. Currently, the leading contenders are Hf-based insulators, with main focus on nitrided Hf-silicate (HfSi$_x$O$_y$N$_z$) [3, 5]. Special attention has been paid to the Si/high-κ interface, since the interface quality fundamentally influences the device performance.

Typically, deposition of metal oxides directly on Si results in formation of an Si-oxide like interfacial layer, as revealed by numerous topographic/imaging techniques, such as medium-energy ion scattering (MEIS), high-resolution transmission electron microscopy (HRTEM) and X-ray photoelectron spectroscopy (XPS) [6]. On atomic scale, this has been prominently demonstrated initially by K-band electron spin resonance (ESR) work [7] on stacks of (100) Si with nm-thick layers of ZrO$_2$ and Al$_2$O$_3$ grown by the atomic layer chemical vapor deposition (ALCVD) method through revealing the presence at the Si/dielectric

interface of Si dangling-bond type point defects (P_{b0}, P_{b1})—the archetypal defects for the (100)Si/SiO$_2$ (SiO$_x$N$_y$) interface. The finding has since been confirmed by various independent ESR studies [8].

As well demonstrated by ESR in conjunction with electrical measurements the P_b-type defects are the dominant class of interface traps invariably introduced at the Si/SiO$_2$ interface as a result of lattice mismatch [9–11]. Their occurrence at the Si/SiO$_2$ interface appears unique. So, in reverse, their presence in Si/high-κ structures is taken as evidence for the presence of an SiO$_{2(x)}$-type interlayer. So far three types of Si dangling-bond-type interface defects have been established by ESR. They correlate with interface orientation, in registry with the crystallinity of the underlying Si substrate. At the (111)Si/SiO$_2$ interface, the only type observed—specifically termed P_b—was identified as trivalent interfacial Si (Si$_3 \equiv$ Si$^\bullet$, where the dot represents an unpaired electron in a dangling Si sp^3 hybrid) backbonded to three Si atoms in the bulk. The technologically favored (100)Si/SiO$_2$ interface exhibits two types, termed P_{b0} and P_{b1}. The experimental evidence is that P_{b0} is chemically identical to P_b, but now residing at microscopically (100)-oriented Si/SiO$_2$ facets. In compliance, both were conclusively established as major systems of detrimental electrical interface traps. The P_{b1} center is assigned to a distorted defected interfacial Si–Si dimer (a $\equiv$ Si–Si$^\bullet$=Si$_2$ defect, where the long hyphen symbolizes a strained bond, with an approximately $\langle 211 \rangle$ oriented unpaired Si sp^3 hybrid). At the (110)Si/SiO$_2$ interface also, only one type, the P_b variant, is observed [9]. Thus all three variants were shown to be interfacial trivalent Si centers, [10, 12, 13] naturally occurring, for standard oxidation temperatures T (800–960 °C), in aerial densities of [P_b] $\sim 5 \times 10^{12}$ cm^{-2} [11] and [P_{b0}], [P_{b1}] $\sim 1 \times 10^{12}$ cm^{-2}.

The presence of an interfacial SiO$_x$ layer in Si/high-κ structures, even though possibly providing the means of realizing standard Si/SiO$_2$ interface quality, is not desirable since the SiO$_2$ layer, of lower κ, impairs the net EOT. Thus, optimization of EOT would mandate to look for a Si/high-κ system without such an SiO$_x$ interlayer. Park and Ishiwara projected that the Si/LaAlO$_3$ structure could be a possible candidate [14] as inferred from depositing the first LaAlO$_3$ thin films (κ = 20–27) on (100)Si using a molecular beam deposition (MBD) method [15]. Later, Edge et al. showed through an intensive study combining Auger electron spectroscopy, infrared absorption, MEIS, HRTEM, and XPS that LaAlO$_3$ films on Si grown by MBD have less than 0.2 Å of SiO$_2$ at the LaAlO$_3$/Si interface [16]. They also showed that these structures have additional

favorable properties such as a 6.2-eV band gap of the LaAlO$_3$ layer and band offsets of (1.8 ± 0.2) eV for electrons and (3.2 ± 0.1) eV for holes [17]. Lu et al. studied amorphous LaAlO$_3$ films deposited on Si by laser molecular beam epitaxy in oxygen containing ambient. Here, HRTEM measurements revealed the presence of an interfacial layer, with thickness increasing with substrate temperature, introduced during film deposition [18]. The LaAlO$_3$ films remained amorphous after post-deposition annealing (PDA) at 1000 °C in N$_2$ or O$_2$, but were found to exhibit a better thermal stability in contact with Si when annealed in an N$_2$ ambient. In a recent paper Sivasubramani et al. reported on a study of amorphous LaAlO$_3$ grown on Si by MBD studied as a function of post-deposition rapid thermal annealing (RTA) for 20 s in flowing N$_2$ [19]. They observed a change in the structure of LaAlO$_3$ from amorphous to polycrystalline after a 935 °C RTA, followed by La and Al penetration into the Si after RTA at temperatures ≥950 °C.

In light of the above results, it appears of much interest to get more in depth information on the true interfacial nature of Si/LaAlO$_3$ structures and the consequences of PDA treatments. The present work deals with an effort to attain structural information on atomic scale by monitoring paramagnetic point defects in (100)Si/LaAlO$_3$ structures with the oxide thin films grown by MBD as a function of the PDA temperature (T_{an}). We will demonstrate, through the occurrence/absence of interface specific (P_{b0}, P_{b1}) and/or interlayer associated (EX) point defects, the appearance, additional thickening and modification of a SiO$_x$ interlayer at $T_{an} \geq 860$ °C. At anneal temperatures up to over 800 °C, the LaAlO$_3$/Si interface is found to be abrupt and thermally stable.

2 Experimental details

2.1 Samples

Details about the samples studied can be found elsewhere [16, 17]. In short, uniform LaAlO$_3$ thin films (10–40 nm) were grown by MBD in an EPI 930 MBE chamber modified for the growth of oxides [20] on Si substrates. The latter were one-side polished commercial 8 inch Si wafers (p-type; $n_a \sim$ (3–6) $\times 10^{15}$ B cm^{-3}). Prior to deposition the native SiO$_2$ on the Si wafers was in situ thermally removed in ultrahigh vacuum at a substrate temperature of 950 °C (as measured with a pyrometer). Subsequently, using elemental sources, La, Al, and molecular oxygen (99.994%) at a background pressure 6×10^{-8} Torr were co-deposited on the sub-

strate at ~100 °C. The La and Al fluxes from the effusion cells were each 2×10^{13} atoms/cm^2 s. As analyzed by Rutherford backscattering spectroscopy, this resulted in closely stoichiometric layers (La:Al mole ratio = 1 ± 0.05).

From these wafers, ESR slices of 2×9 mm^2 main area were cut with their 9-nm edge along a $\langle 0\bar{1}1 \rangle$ direction. Cutting damage was removed through selective chemical etching of backside and edges. Thermal stability of deposited LaAlO$_3$ layers and interfaces was analyzed by subjecting samples to ~10 min post-deposition heating at desired temperatures between 630 and 1000 °C generally in a 1 atm N$_2$ + 5% O$_2$ (99.995%) ambient or pure N$_2$ (99.999%) using a conventional resistively heated laboratory facility. Several sets of samples were used for the various thermal steps. As an additional test related to potential ESR activation/maximalization of diamagnetic defects some samples were subjected for ~10 s to 10.02 eV vacuum UV photons (flux ~5×10^{14} cm^{-2} s^{-1}) obtained from a Kr resonant discharge lamp or to short positive corona charging (3 μA for 10 s) in room ambient.

2.2 Electron spin resonance

Conventional cw slow-passage K-band ESR measurements were carried out at 4.2 K, as described elsewhere, [11] for the applied magnetic field **B** rotating in the $(0\bar{1}1)$ Si substrate plane over an angular range $\Phi_B = 0\text{–}90°$, with respect to the [100] interface normal **n**. A co-mounted Si:P reference sample of $g(4.2 \text{ K}) = 1.99869 \pm 0.00002$ was used for g factor and spin density calibration, with the latter performed through orthodox double numerical integration of the detected derivative-absorption spectra dP_μ/dB, where P_μ is the incident microwave power. (For more details, see Ref. [11]). The attained absolute and relative accuracy is estimated at ~30% and ~10%, respectively. Typically, an ESR sample was comprised of 10–12 slices HF (5% in H$_2$O) dipped immediately before taking ESR data.

3 Results and analysis

Figure 1 presents an overview of representative ESR spectra, observed with **B**//**n** on the as deposited (100)Si/LaAlO$_3$ structures and after different PDA steps. Within spectral accuracy, no ESR active defects could be observed on the as grown samples, the situation remaining unaltered for annealing up to $T_{an} \leq 800$ °C.
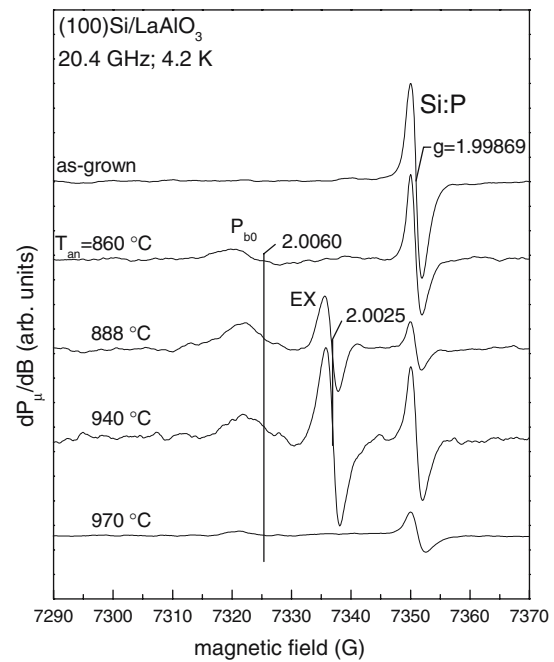

Fig. 1 Representative derivative-absorption K-band ESR spectra measured at 4.2 K with applied magnetic field **B** perpendicular to the interface of (100)Si/LaAlO$_3$ structure subjected to different steps of post-deposition annealing in N$_2$ + 5% O$_2$ (10 min). Spectral heights have been normalized to equal marker intensity and sample area. The applied modulation field amplitude B$_m$ was 0.6 G, and incident P_μ ~ 2.5 nW. The signal at $g = 1.99869$ stems from a co-mounted Si:P marker sample

However, upon annealing in the temperature range T_{an} ~ 860–970 °C, a resonance signal is observed at zero crossing $g = 2.0060 \pm 0.0001$ with $\Delta B_{pp} = (7 \pm 1)$ G, exhibiting distinct angular anisotropy. To trace the signal's origin, a coarse g map was composed for **B** rotating in the $(0\bar{1}1)$ plane. As shown in Fig. 2, the obtained data could be well fitted by an axial symmetric system (cf. solid curves in Fig. 2) with principal g values $g_{\parallel} = 2.0017 \pm 0.0001$ and $g_{\perp} = 2.0082 \pm 0.0001$. These results match those obtained for the g pattern of the P$_{b0}$ defect in standard thin SiO$_2$/Si systems [13], indicating that the currently observed center concerns the P$_{b0}$ defect. Interestingly, one more signal becomes observable after annealing in the range T_{an} ~ 888–940 °C, as can be seen in Fig. 1. It concerns an isotropic signal observed at $g = 2.0025 \pm 0.0001$, which as can be noticed in Fig. 1 and as clearly revealed by more focused optimized ESR observations, appears accompanied by a hyperfine doublet (~16.4 G splitting) centered on this g value. These ESR parameters are characteristic for the EX defect, [21] an SiO$_2$ associated center, well known from studies of bulk SiO$_2$ and Si/SiO$_2$ structures [22].
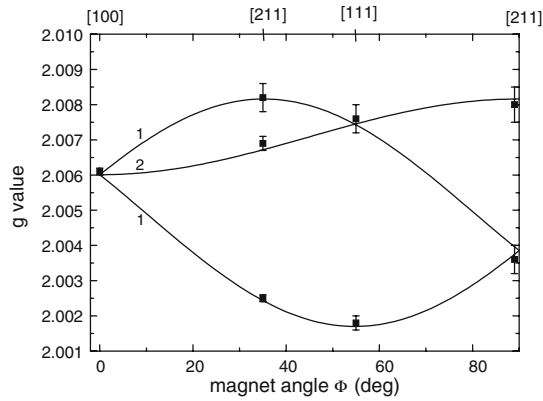
Fig. 2 Coarse angular g map of the observed resonances, ascribed to P_{b0} for **B** rotating in the $(0\bar{1}1)$ plane with respect to the interface normal **n** observed in a $(100)Si/LaAlO_3$ structure subjected to a post-deposition anneal at 900 °C for ~10 min. The curves represent the optimized fitting of the various branches for axial symmetry yielding $g_{\parallel} = 2.0017 \pm 0.0001$ and $g_{\perp} = 2.0082 \pm 0.0001$, within experimental accuracy in agreement with the P_{b0} data for standard thin thermal oxide/Si structures, affirming the P_{b0} assignment. The added numbers indicate relative branch intensities expected from the standard defect model, also matching experimental observation

In the as deposited and PDA treated samples, no LaAlO$_3$-specific point defects could be observed. Most probably point defects are present but residing in a diamagnetic state, making them invisible for ESR detection. So, in an improving effort, to maximally reveal defects in the oxides as well as at the interface, the samples were subjected to additional VUV irradiation. The VUV irradiation has been demonstrated to be a most efficient method, for both oxide and interface defects in Si/SiO$_2$, to photo-dissociate H-terminated dangling bonds and possibly additionally unveil weak or strained bonds [7]. Along the same lines, to put possibly occurring diamagnetic defects in the LaAlO$_3$ films in the correct charge state for ESR detection, some samples were additionally subjected to positive corona charging in room ambient, only applied for a very short time though in order to avoid marring H-related aberrations inherent to such method [23]. Yet, the observed spectra remained unaffected. So, in spite of these efforts, no LaAlO$_3$ related defects could be observed. Though disappointing, the result is not entirely negative: It importantly indicates that no P$_b$-type defect system has remained (partially) hidden as a result of inadvertent passivation, as could be expected from the H-free fabrication process of the samples.

4 Interpretation and discussion

The occurring point defects in the $(100)Si/LaAlO_3$ structures were monitored as a function of PDA

treatment, additional VUV irradiation and corona charging. The main results are compiled in Fig. 3 showing the inferred density of the observed defects as a function of PDA temperature for PDA in a 5% O$_2$/N$_2$ mixture. These results reveal several noteworthy items, perhaps most interesting of all, as will appear, information on annealing induced structural/compositional changes in the interface region. As mentioned, there have previously been carried out morphological/compositional studies [15, 16, 18, 19] on the Si/LaAlO$_3$ entity, from where, in fact, it was concluded this entity to concern a remarkable structure. So, it seems obvious to compare the currently acquired information on atomic level with the results gathered from combined structural/imaging studies. Though perhaps a bit unusual, it is this comparison that will guide the discussion and interpretation of the thermal evolution of the observed defect densities as compiled in Fig. 3. To ease the comparison, we recall that, in particular, one recent work [19] has analyzed the thermal stability of $(100)Si/LaAlO_3/Al_2O_3$ stacks as a function of RTA in N$_2$ ambient over the range 850–1040 °C for 10–20 s. Using atomic force microscopy (AFM) and X-ray diffraction (XRD), the work reports that RTA from 900 °C onward starts to generate changes in surface morphology, together with the initiation of the amorphous to polycrystalline transformation of the LaAlO$_3$ film. Secondary-ion-mass spectroscopy (SIMS) analysis unveils substantial penetration of La and Al atoms into
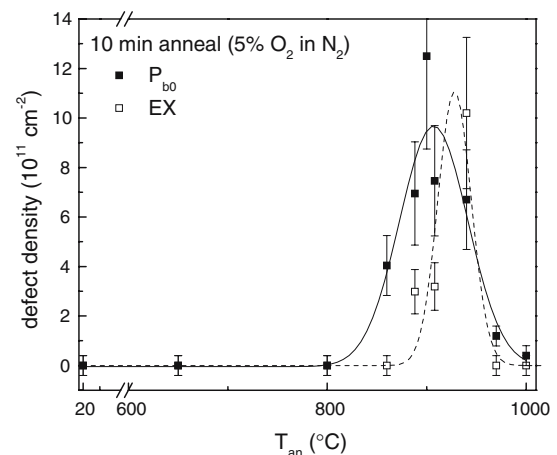

Fig. 3 Compilation of the inferred defect densities in $(100)Si/LaAlO_3$ entities as a function of the post-deposition isochronal annealing in N$_2$ + 5% O$_2$ (10 min) for P_{b0} and EX centers, represented by closed and open symbols, respectively. The solid and dashed traces are Gaussian curves, merely meant to guide the eye in exposing the peaking in defect generation and the somewhat lagging behind (~30 °C) of EX production vis-à-vis P_{b0} appearance. Data points at zero defect density symbolize failure of signal detection

the underlying Si substrate for RTA at or above 950 °C, with, however, any effect of penetration remaining below the detection limit for T_{an} kept below ~935 °C.

We now turn to Fig. 3: In the as deposited (100)Si/LaAlO$_3$ structure no ESR active defects could be observed, which situation did not change upon VUV irradiation. For the P$_b$-type interface defects in Si/SiO$_2$ structures it has been demonstrated that this treatment efficiently dissociates H-passivated Si bonds. The non observation of the inherent dangling bond-type Si/SiO$_2$ interface defects in the as deposited (100)Si/LaAlO$_3$ structure indicates the absence of an Si/SiO$_2$-type interface, i.e., there is no SiO$_x$-type interlayer present or this interlayer is at least thinner than 3 Å [24]. This result is in good agreement with previous HRTEM measurements indicating that the as-deposited La-AlO$_3$/Si structure has less than 0.2 Å of SiO$_2$ at the interface [16]. The absence of an SiO$_x$-type interlayer in the LaAlO$_3$/Si structures is quite dissimilar from what is encountered in other Si/high-κ structures such as ZrO$_2$/Si, HfO$_2$/Si, and Al$_2$O$_3$/Si, where, as also borne out by ESR studies, the presence of such an interlayer appears symptomatic, even in the as-fabricated state [7, 8]. The abrupt interface remains unaltered even during subsequent annealing up to $T_{an} \leq 800$ °C, indicating that the interface is thermally stable.

Upon annealing at T_{an} ~ 860 °C an anisotropic ESR center appears that could be identified as the P$_{b0}$-type defect. By its uniqueness, the occurrence of this interface defect quite convincingly signals the presence of a Si/SiO$_{(x)2}$-type interface, viz., an SiO$_x$-type interlayer has formed in the LaAlO$_3$/Si structure. Upon annealing at a slightly higher temperature T_{an} ~ 888 °C another defect is observed—so lagging behind by ~30 °C in terms of T_{an}—identified as EX, an SiO$_2$-associated center. The presence of this defect center does not only attest to the presence of an SiO$_x$ interlayer, but also indicates an additional growth or modification of the interlayer. Indeed, the defect was not observed in the sample annealed at T_{an} ~ 860 °C even though the presence of an SiO$_x$-type interlayer in this sample is evidenced by the observation of P$_{b0}$-type defects. It suggests that a minimal thickness of the SiO$_x$ interlayer is needed to enable formation of EX defects sufficient for ESR detection, at least more substantial than required for effective Si/SiO$_2$ interface formation. Thus, while affirming the presence of an SiO$_{2(x)}$ interlayer, its retarded appearance indicates an additional growth (or modification) of the interlayer. The thickness of the interlayer, however, is unknown. In comparison with previous data, the initiation of the

formation of a Si/SiO$_x$-type interface might be linked with the very embryonic state of the onset of LaAlO$_3$ crystallization observed in a previous work [19], which is then followed by some more substantial SiO$_{2(x)}$-type interlayer growth as T_{an} is increased.

The defect density versus T_{an} curves (Fig. 3) show a peaked behavior, simulated by Gaussian curves. The maximum P$_{b0}$ density, [P$_{b0}$] ~ $(1.3 \pm 0.3) \times 10^{12}$ cm^{-2}, is obtained at $T_{an} = 900$ °C while the maximum EX density [EX] ~ $(1.0 \pm 0.3) \times 10^{12}$ cm^{-2}, is obtained at a slightly higher PDA temperature $T_{an} = 940$ °C. Based on the P$_{b0}$ occurrence, it appears that for annealing from $T_{an} > 900$ °C onward the interface starts to break up. Yet, it is interesting to note that in the range T_{an} ~ 900–940 °C, the EX density still increases while the P$_{b0}$ density already starts to decrease. So, the structural changes breaking up the interlayer seem to first affect the P$_{b0}$ defects located at the interface before they affect the interlayer associated defects EX. Former studies have shown that a RTA at 900 °C induces changes in the morphology of the lanthanum aluminate [19]. Atomic force microscopy and X-ray diffraction measurements revealed the transition from an amorphous network to a polycrystalline LaAlO$_3$ network at $T_{an} = 935$ °C.

Upon annealing at elevated temperatures $T_{an} > 940$ °C, it is seen that the P$_{b0}$ as well as the EX defect density decrease abruptly. Both types of defects rapidly disappear altogether, pointing out that the SiO$_{2(x)}$ character of the interlayer is destroyed. It is at about this RTA temperature ($T_{an} = 950$ °C, 20 s) that back side SIMS profiling shows a substantial penetration of LA and Al into the Si substrate [19]. This in(ter)diffusion seems to chemically disrupt the pristine nature of the SiO$_x$ component (possibly silicate formation) resulting in the annihilation of the SiO$_{2(x)}$-specific point defects. It is possible that the onset temperature for La and Al outdiffusion in the current case is somewhat lower considering the longer PDA treatment times (10 min) as compared to previous work applying RTA for 10–20 s.

In comparing data, it comes as a general impression that ESR seems to sense thermally induced changes in the Si/LaAlO$_3$ entities ''before'' the impressive arsenal of profound structural/morphologic studies do, i.e., at lower T_{an}. In fairness, this may partly be the result from the applied larger anneal times in the current work possibly reinforced by the addition of O$_2$ to the anneal ambient (5% O$_2$ in N$_2$). Yet, while possibly partially true, in a different view pointing to the probing on the atomic level, it may as well bear out the attribute of ESR as prone to detect interfacial reshaping in a very embryonic state, before

standard compositional/imaging techniques. The latter seems to find support from additional ESR work on samples subjected to PDA steps at similar anneal temperatures and times in pure N_2 (99.9999%), generally leading to similar results as obtained for the O_2/N_2 ambient.

The P_{b0}-type defects observed indicate that a Si/SiO_2-type interface has formed. As demonstrated, the obtained ESR parameters such as g-value, line width and defect density are indeed very similar to those characteristic for thermal Si/SiO_2 interfaces. There is, however, one remarkable apparent dissonance: No P_{b1} ($g_1 = 2.00577$, $g_2 = 2.00735$, $g_3 = 2.0022$) centers could be detected. The P_{b1} center also concerns an unpaired sp^3 hybrid at a threefold Si atom part of a strained Si–Si dimer ($\equiv Si–Si^{\bullet}=Si_2$), thus basically chemically identical to the P_{b0} center, yet physically different, e.g., regarding hybrid orientation, bond strain, and structural relaxation [12]. Standard, the P_{b0} and P_{b1} centers are almost invariably observed in tandem at the $(100)Si/SiO_2$ interface, although relative intensities may vary. So, the question arises as to the absence of the P_{b1} defect, at least below ESR sensitivity, at the current $Si/SiO_{2(x)}$-type interface formed during PDA of $(100)Si/LaAlO_3$ entities. The reason for this is presently still unclear. Yet, for reference, it may be added that low densities of P_{b1} defects (relatively to P_{b0}) in some types of $(100)Si/SiO_2$ interfaces have been observed before [25].

5 Summary

In summary, it is found that the $(100)Si/LaAlO_3$ structure exhibits a nominally "perfect" interface in terms of dangling-bond-type interface defects, which can endure extended thermal anneals up to ~800 °C. Yet, upon annealing at $T_{an} \geq 860$ °C an SiO_x-type interlayer is formed as evidenced by the appearance of P_{b0}-type defects. This interlayer formation is possibly linked with the onset of crystallization of the amorphous $LaAlO_3$ film. At somewhat higher T_{an} the EX defect is observed by ESR. The "delay" of the appearance of EX in terms of T_{an} indicates an additional growth of the interlayer. However, upon annealing at temperatures $T_{an} \geq 908$ °C, the Si/SiO_2 character of the interlayer starts to break up to get rapidly eradicated with T_{an} increasing to ≥ 960 °C, as evidenced by the disappearance of the P_{b0} and EX centers altogether. This evanescence of the $SiO_{2(x)}$ character of the interlayer is ascribed to La and Al penetration into the Si substrate, finally possibly resulting in silicate (interlayer) formation.

Generally, the obtained results are in compliance with previous results obtained from morphological/imaging methods, also reporting that RTA from about 900 °C onward starts to induce changes in surface morphology accompanied by the transformation of the amorphous to the polycrystalline state of the superficial $LaAlO_3$ film. However, by deepening in towards atomic detail using specific ESR-monitored defect diagnosis, the occurrence of a $Si/SiO_{2(x)}$ type interface over a certain T_{an} span during the interfacial evolution of the interface as a function of applied PDA is additionally unveiled. This interfacial reshaping appears detected in an early embryonic state ahead, in terms of T_{an}, of any alterations observed by state-of-the art morphological/imaging methods.

Thus, the analysis confirms the potential of sensitive ESR analysis to unveil elemental aspects of evolving semiconductor/insulator interfaces (structures) on the atomic level. The tool complements the state-of-the-art morphological/imaging methods on true atomic level.

References

1. G.D. Wilk, R.M. Wallace, J.M. Anthony, J. Appl. Phys. **89**, 5243 (2001)
2. M. Houssa, L. Pantisano, L.-Å. Ragnarsson, R. Degraeve, T. Schram, G. Pourtois, S. De Gendt, G. Groeseneken, M.M. Heyns, Mat. Sci. Eng. **R51**, 37 (2006)
3. See *The International Technology Roadmap for Semiconductors*, 2005 ed. (Semiconductor Industry Association, San Jose, CA, 2005)
4. M.A. Quevedo-Lopez, M. El-Bouanani, B.E. Gnade, R.M. Wallace, M.R. Visokay, M. Douglas, M.J. Bevan, L. Colombo, J. Appl. Phys. **92**, 3540 (2002)
5. J. Robertson, Eur. J. Appl. Phy. **28**, 265 (2004)
6. See, e.g., W. Vandervorst, B. Brijs, H. Bender, O. T. Conrad, J. Petry, O. Richard, S. Van Elshocht, A. Delabie, M. Caymax, S. De Gendt, Mat. Res. Soc. Symp. Proc. **745**, 23 (2003)
7. A. Stesmans, V.V. Afanas'ev, J. Phys.: Condens. Matter. **L673**, 13 (2001); Appl. Phys. Lett. **80**, 1957 (2002)
8. J.L. Cantin, H.J. von Bardeleben, J. Non-Cryst. Solids. **303**, 175 (2002); S. Baldovino, S. Nokrin, G. Scarel, M. Fanciulli, T. Graf, M.S. Brandt, J. Non-Cryst. Solids. **322**, 168 (2003); A.Y. Kang, P.M. Lenahan, J.F. Conley Jr., R. Solanski, Appl. Phys. Lett. **81**, 1128 (2002); B.J. Jones, R.C. Barklie, Microelectron. Eng. **80**, 74 (2005)
9. R. Helms, E.H. Poindexter, Rep. Prog. Phys. **57**, 791 (1994)
10. K. Brower, Phys. Rev. B **38**, 9657 (1988)
11. A. Stesmans, Phys. Rev. B **48**, 2418 (1993)
12. A. Stesmans, B. Nouwen, V.V. Afanas'ev, Phys. Rev. B **58**, 15801 (1998)
13. A. Stesmans, V.V. Afanas'ev, J. Appl. Phys. **83**, 2449 (1998)
14. B.E. Park, H. Ishiwara, Appl. Phys. Lett. **79**, 806 (2001)
15. B.E. Park, H. Ishiwara, Appl. Phys. Lett. **82**, 1197 (2003)
16. L.F. Edge, D.G. Schlom, R.T. Brewer, Y.J. Chabal, J.R. Williams, S.A. Chambers, C. Hinkle, G. Lucovsky, Y. Yang, S. Stemmer, M. Copel, B. Holländer, J. Schubert, Appl. Phys. Lett. **84**, 4629 (2004)

17. L.F. Edge, D.G. Schlom, S.A. Chambers, E. Cicerrella, J.L. Freeouf, B. Holländer, J. Schubert, Appl. Phys. Lett. **84**, 726 (2004)
18. X.B. Lu, X. Zhang, R. Huang, H.B. Lu, Z.H. Chen, W.F. Xiang, M. He, B.L. Cheng, H.W. Zhou, X.P. Wang, C.Z. Wang, B.Y. Nguyen, Appl. Phys. Lett. **84**, 2620 (2004)
19. P. Sivasubramani, M.J. Kim, B.E. Gnade, R.M. Wallace, L.F. Edge, D.L. Schlom, H.S. Craft, J.P. Maria, Appl. Phys. Lett. **86**, 201901 (2005)
20. J. Lettieri, J.H. Haeni, D.G. Schlom, J. Vac. Sci. Technol. A **20**, 1332 (2002)
21. A. Stesmans, Phys. Rev. B **45**, 9502 (1992); A. Stesmans, F. Scheerlinck, Phys. Rev. B **50**, 5204 (1994); J. Appl. Phys. **75**, 1047 (1994)

22. A. Baumer, M. Stutzmann, M.S. Brandt, F.C.K. Au, T.S. Lee, Appl. Phys. Lett. **85**, 943 (2004); W.E. Carlos, S.M. Prokes, J. Appl. Phys. **78**, 2129 (1995); M. Dohi, H. Yamatani, T. Fujita, J. Appl. Phys. **91**, 815 (2002)
23. A. Stesmans, V.V. Afanas'ev, Appl. Phys. Lett. **82**, 2835 (2003)
24. W. Futako, T. Umeda, M. Nishizawa, T. Yasuda, J. Isoya, S. Yamasaki, J. Non-Cryst. Solids. **575**, 299–302 (2002)
25. A. Stesmans, V.V. Afanas'ev, Appl. Phys. Lett. **77**, 1469 (2000)